

Electronic transport, structure, and energetics of endohedral Gd@ C_{82} metallofullerenes

L. Senapati, J. Schrier, and K. B. Whaley

*Department of Chemistry and Pitzer Center for Theoretical Chemistry,
University of California, Berkeley, CA 94720-1460, USA.*

Electronic structure and transport properties of the fullerene C_{82} and the metallofullerene Gd@ C_{82} are investigated with density functional theory and the Landauer-Buttiker formalism. The ground state structure of Gd@ C_{82} is found to have the Gd atom below the C-C bond on the C_2 molecular axis of C_{82} . Insertion of Gd into C_{82} deforms the carbon chain in the vicinity of the Gd atoms. Significant overlap of the electron distribution is found between Gd and the C_{82} cage, with the transferred Gd electron density localized mainly on the nearest carbon atoms. This charge localization reduces some of the conducting channels for the transport, causing a reduction in the conductivity of the Gd@ C_{82} species relative to the empty C_{82} molecule. The electron transport across the metallofullerene is found to be insensitive to the spin state of the Gd atom.

I. INTRODUCTION

Endohedral metallofullerenes¹ have attracted wide interest due to their functional characteristics and potential applications in the field of nanomaterials and biomedical science.² Recently, metallofullerene doped nanotubes ("peapods") have also attracted experimental attention due to their structural and electronics properties,^{3,4,5} and have been proposed as a possible self-assembled quantum computing architecture.⁶ Additionally, recent experimental studies of Gd@ C_{82} in single wall carbon nanotube ((Gd@ C_{82})@SWNT) peapods have shown novel transport behavior.⁷ The first step in understanding the properties of the peapod structures is an adequate treatment of the individual Gd@ C_{82} fullerenes.

In earlier Gd@ C_{82} theoretical calculations by Kobayashi and Nagase,⁸ the relaxation of the fullerene cage was not considered, nor the possibility of novel geometries for the Gd atom in the fullerene cage was not considered; the predicted ground state spin multiplicity $M = 9$, resulting from ferromagnetic coupling between the Gd f-electrons and the odd electron on the fullerene cage, is in contrast to electron spin resonance determinations of a $M=7$ ground state, due to antiferromagnetic coupling of -1.8 cm^{-1} .⁹ The $M=7$ ground state is also supported by magnetic studies.^{10,11,12,13} In order to resolve this discrepancy, we present results of density functional calculations for the equilibrium geometries, magnetic and transport properties of Gd@ C_{82} , made with the Landauer-Buttiker transport formalism. Section II gives

a brief description of the theoretical procedure, Section III present our results, and Section IV draws conclusions and discusses possible future directions.

II. COMPUTATIONAL METHODS

The equilibrium geometry and the total energy of Gd@ $\text{\AA}2$ are calculated using density functional theory (DFT).¹⁴ One of the primary considerations involved in these calculations is determination of a suitable basis set and exchange correlation functional. We therefore compared the bond length, binding energy and spin multiplicity values of Gd and Gd dimer (Gd_2) optimized using several different basis sets and exchange correlation functionals, to experimental values¹⁵ and theoretical all-electron relativistic calculations¹⁶. As we discuss in Section III A, the results are quite sensitive to the choices of both basis set and exchange correlation functional. A relativistic effective core potential CEP-121G¹⁷ for the atoms with the generalized gradient approximation of Becke's exchange functional¹⁸ and Lee-Yang-Parr correlational functional¹⁹ (B3LYP) gave results comparable to experiment, and were thus used for the subsequent calculations.

The total energies and forces are calculated using the linear combination of atomic orbitals (LCAO) molecular orbital approach.¹⁴ We employed a 6-31G basis for the carbon atoms and a CEP-121G basis set for Gd. The computations were performed using Gaussian03 for various spin multiplicities.²⁰ The geometries were optimized without symmetry constraints by minimizing the total energy and requiring the forces to vanish within a 10^{-3} a.u./Bohr threshold, at every atom site. To find the ground state structure for Gd@ $\text{\AA}2$, initial positions of the Gd atom inside the $\text{\AA}2$ cage were generated, then optimized without constraining any of the atomic coordinates. The calculations were repeated for different spin multiplicities to determine the ground state spin configuration, as we discuss in Section III B. Although the partitioning of charge to specific atoms or groups within a molecule is not uniquely defined within the postulates of quantum mechanics,²¹ a recent experimental evaluation of density functional charge schemes²² found the commonly used Mulliken charge analysis²¹ to be generally deficient for charge calculations, and Natural Population Analysis²³ (NPA) to be the most generally accurate method of those studied.

To study the transport, we created a model comprised of $\text{\AA}2$ located between two Au contacts, with and without the endohedral Gd atom. The numbers of Au atoms on each side of the contact were varied to study the transport dependence on contact geometry. Fig.1 shows one of these structures with a triangular contact of 3 Au layers in which the layer adjacent to $\text{\AA}2$ has one Au atom, the second has 3 Au atoms and the third layer has 6 Au atoms. For calculation of electron transport through Gd@ $\text{\AA}2$ and $\text{\AA}2$, we used the non-equilibrium Green's function based

Landauer-Buttiker formalism.^{24,25,26} Neglecting spin-flip processes, the total current due to coherent scattering is given by $I_{spin-coherent}=I^\alpha + I^\beta$, where I^α and I^β are the contribution to current from spin up (α) and down (β) states, respectively. The spin specific contributions are expressed as the integral over the injection energy of the tunnelling electron, E ,

$$I^{\alpha(\beta)} = (e/h) \int_{\mu_2}^{\mu_1} T^{\alpha(\beta)}(E, V) [f(E, \mu_1) - f(E, \mu_2)] dE, \quad (1)$$

taken between the electrochemical potentials μ_1 and μ_2 ,

$$\mu_1 = E_f - (q_1 V / (q_1 + q_2)) \quad (2)$$

$$\mu_2 = E_f + (q_2 V / (q_1 + q_2)), \quad (3)$$

where q_1 and q_2 are charge accumulated in the left and right contacts respective, V is the applied bias, and E_f is the Fermi energy of the gold contact, taken as -5.53 eV for our calculation. $f(E, \mu)$ is the Fermi distribution function and $T^{\alpha(\beta)}(E, V)$ is the transmission function that represents the sum of transmission probabilities for electrons of a given spin through the contact/metallofullerene complex, obtained from the overlap and Hamiltonian matrices determined by the DFT calculation. The explicitly included Au atoms in our model system described above are used to obtain the coupling matrices for calculation of self-energy functions.^{24,26} We have used the local density of states of the 6s-band of bulk gold (0.035 eV per electron spin) to approximate the Green's function of the (bulk) Au contact.²⁶

III. RESULTS

A. Properties of Gd and Gd₂

First, we discuss the geometry, ionization potential, and electron affinity of Gd and Gd₂ and compare these with experiment. This comparison is provided to assess the accuracy of our theoretical procedure.

To assess how well our method accounts for the properties of the Gd atom, we have calculated the ionization potential of Gd and Gd₂ as well as the binding energy and Gd₂ dimer bond length. The ground state Gd atom was found to have a spin multiplicity of 9 for all functionals that we have considered with the CEP-121G effective core potential basis functions.¹⁷ Results for the LSDA,¹⁴ B3LYP^{18,19} and PW91²⁷ functionals are presented in Supplemental Table I. The calculated binding energy value (1.7595 eV) and bond-length (2.926 Å) for Gd₂ with CEP-121G as frozen core basis function and B3LYP as functional for spin multiplicity of 19 agrees well with the experimental binding energy (1.784±0.35 eV)¹⁵ and the relativistic all-electron theoretical bond-length (2.895 Å)¹⁶. The ionization potential for

Gd and Gd₂ were calculated as 5.014 eV and 4.119 eV respectively. Based on these results, the CEP-121G basis set for Gd and 6-31G basis set for C atoms, together with the B3LYP functional, were used for the Gd@C₈₂ calculations.

Although we have employed a frozen core, the Gd 5s and 5p core electrons are allowed to relax in the molecular calculations. Atomic calculations show that the relaxation of these states is often crucial for an accurate determination of valence state properties because of the overlap of the 5d electron orbitals with the other n=5 orbitals.

B. Structure of Gd@ C_{82}

We have taken a C_{82} fullerene cage with C_{2v} point group symmetry $\text{C}_{2v}(\text{C}_{2v})$ and optimized the structure with Gd inside at various positions, as described in Section II. In the $\text{C}_{2v}(\text{C}_{2v})$ fullerene cage, the C_2 -axis goes through the center of one six-membered ring and one C-C double bond. Our calculations reveal that the ground state structure of Gd@ C_{82} has the Gd atom situated adjacent to the C-C double bond on the symmetry axis, as shown in Fig. 2. This is in contrast to reported results for other metal atoms such as Sc, Y and La in C_{82} ,^{8,28,29,30,31,32} where the metal atoms are found to be centered inside the fullerene cage on top of the C_{2v} axis six-membered ring.^{8,29} Recent synchrotron radiation powder structure analysis experiments of Gd@ C_{82} are consistent with our calculated placement of the Gd atom.³³ The distances between Gd and the two nearest C atoms are 2.38 Å and 2.41 Å respectively. The binding energy of Gd to C_{82} is found to be 5.6435 eV (130.1 kcal/mole), comparable to those for the Sc, Y, and La metallofullerenes;⁸ the energy levels of C_{82} and Gd@ C_{82} are shown in Supplemental Figure 1. Addition of Gd into C_{82} slightly lengthens the proximal C-C bond (from 1.425 Å to 1.473 Å) atom, as well as the neighboring C-C bonds (by 0.01 to 0.04 Å). This deformation results in an energy difference between the $\text{C}_{2v}(\text{C}_{2v})$ symmetry structure and the Gd@ C_{82} optimized deformed structure when recalculated without Gd of 0.109 eV (2.51 kcal/mole).

As discussed in Section II, the NPA charge partitioning tends to give better results; our Gd@ C_{82} calculations agree with this analysis, as the Mulliken charge analysis indicates charge transfer of 1.43 electrons from Gd atom to the C_{82} cage, and NPA indicates a charge transfer of 2.43 electrons. The latter value agrees well with electron energy loss spectroscopy (EELS) experiments.³⁴ The electrons are localized near the two proximal carbon atoms, resulting in strong charge density overlap between the Gd atom and these C atoms. NPA analysis also gives a Gd *d*-orbital population of 0.48 electrons, consistent with a Dewar-Chatto back-bonding interaction between the Gd atom and the carbon double bond.³⁵ The deformation of the C-C bonds near the Gd is also consistent with back-bonding, as the back donation of charge from the C-C bonds to the d-orbitals weakens (and hence lengthens) the bonds. Additionally, the Gd *f*-orbital population of 7.02 is consistent with the charge transfer from the cage of 0.04 electrons empirically

determined by Nádai *et al.* for reproducing X-ray magnetic circular dichroism experiments.³⁶

In order to study the difference in Gd placement, as compared to the Sc, Y, and La cases, we performed single point calculations, in which the Gd atom was placed in the La-like position, adjusting the distance between the hexagon and the Gd atom to account for the smaller radius of the Gd^{+3} ion as compared to the La^{+3} ion;³⁷ The lowest total energy structure we found occurred when the Gd atom was placed 2.10 Å above the plane of the hexagon; this structure had a total energy of 0.104 hartrees (2.83 eV) higher than the ground position determined by our optimizations. NPA analysis determined nearly identical charge distribution on the Gd atom in both cases, attesting to the importance of Gd-C back-bonding in stabilizing the structure. However, an elementary electrostatic analysis, using the NPA atomic charges as point ions, gives a Gd-cage potential energy of -1.015 and -0.9366 hartrees for the ground and La-like positions respectively; the difference between these nearly accounts for the difference in total energies. This interpretation is consistent with resonant photoemission spectroscopy experiments which suggest that the Gd-C bond is primarily ionic in character.³⁸

We have also examined the effect of different spin configurations on the optimized the $\text{Gd}@82$ structure. The ground state structure was found to have 7 unpaired electrons on Gd and one unpaired electron on the 82 cage aligned antiparallel to the Gd spins, with total spin multiplicity $M=7$, in agreement with magnetic studies.^{10,11,12,13} The next lowest energy structure has $M=9$, with seven unpaired electrons at Gd and the odd 82 cage electron oriented parallel to the Gd spins. The energy difference between these two configurations is 2.6 meV (16.1 cm^{-1}), which compares favorably to the experimentally determined value of 14.4 cm^{-1} .⁹ The detailed energies with various spin multiplicities are listed in Table I.

C. Electronic transport

In order to see the effects of contact geometry, we have taken between one and three layers of Au atoms to represent the contact. To obtain the contacts, single Au atoms were placed on each side of the $\text{Gd}@82$ molecule, shown schematically in Fig. 1, at a distance of 2.015 Å from the carbon atoms, along the C_{2v} symmetry axis. To build the larger contacts, the bond lengths and geometry of bulk Au were used to add 3 Au atoms to the second layer and 6 Au atoms to the third layer, as shown in Fig. 1. Although it is known that the conductance can be strongly dependent on the contact structure,³⁹ this transport model serves as the basis for understanding the qualitative transport properties of $\text{Gd}@82$.

Calculated I-V characteristics for 82 and $\text{Gd}@82$ with various spin states and Au contact geometries are shown in

Figs. 3, 4, 5, and Supplemental Fig. 3. The ground state ($M=7$) transport with a single Au atom contact on each side of the fullerene is shown in Fig. 3. Addition of the Gd atom into the C_{82} cage leads to a reduction in the current. To understand this difference, we computed the density of state (DOS) for both structures, and found the metallofullerene to have a reduced DOS near the Fermi energy as compared to C_{82} . These results are shown in Supplemental Fig. 2. The I-V characteristics for the two- and three-layer contact structures were found to be qualitatively the same as for the single Au atom contact case, and are shown in Supplemental Fig. 3 and Fig. 4, respectively. Quantitatively, the current is seen to increase with the addition of further gold layers, due to the increasing number of conduction channels.

Calculations for the $M=9$ structure, which is structurally degenerate to the $M=7$ system, are shown in Fig. 5. We find only a small difference in current between the two spin configurations, and the conduction properties of spin up and spin down electrons (as calculated in Eq.(1)) were found to be insensitive to the Gd spin configurations, suggesting that the spin of the Gd is shielded by the cage carbon atoms and that transport occurs consequently only through the fullerene cage. This is also supported by plots of the highest occupied and lowest unoccupied molecular orbitals (HOMO/LUMO), shown in Figs. 6 and 7, which indicate that conduction occurs primarily through the C_{82} cage and shows no signature of conducting paths involving the Gd atom. This suggests that incorporation of Gd decreases the number of available conduction channels between the contacts, as a result of the charge localization effect noted in Section III B.

By attaching the Au contacts, one expects some charge transfer from the metallic contact to the fullerene at zero bias, but this effect (which is the same for both structures) is relatively small due to the weak coupling between the fullerene and metal contact. Using the NPA method described in the previous section, the charge transfer from the left and right Au contacts to the C_{82} cage were found to be 0.09 and 0.11 electrons for single layer of Au, 0.12 and 0.13 electrons for the two layer contact and 0.13 and 0.15 electrons for the three layer contact. Use of these charge values in the expression for the electrochemical potential, Eq.(2), had no effect on the calculated transport properties. Despite the fact that Gd is closer to one of the electrodes, we observed no diode like behavior; we attribute this to the the conduction occurring primarily through the fullerene cage, which is approximately symmetrical with respect to both contacts.

IV. CONCLUSIONS

We have analyzed the energetics, structure, and transport properties of Gd@ $\text{\AA}2$. The present results indicate that the CEP-121G basis set for Gd, with the B3LYP density functional for exchange and correlation, is a satisfactory combination for DFT calculations for large Gd endofullerene systems. Our calculated structure for Gd@ $\text{\AA}2$ confirms the geometry determined by x-ray diffraction data, indicating that the Gd is located adjacent to the C-C double bond on the symmetry axis, in contrast to the other Group-3 metallofullerenes. Furthermore this geometry gives calculated spin configurations that agree with ESR and magnetic experiments, in contrast to previous theoretical studies. Using the Landauer-Buttiker formalism for transport, we find that conduction occurs primarily through the $\text{\AA}2$ cage, and that charge donation from the Gd atom to the cage disrupts these conduction channels. We find no evidence for electron-spin dependent transport effects due to the spin state of the Gd atom. Besides providing a solid methodological and structural basis for future calculations of (Gd@ $\text{\AA}2$)@SWNT structures, the absence of HOMO/LUMO density on the Gd atom—and thus relative lack of interaction with the surrounding nanotube—helps explain why the M_4 and M_5 peak edges of the (Gd@ $\text{\AA}2$)@SWNT EELS spectrum were found to be identical to that for Gd@ $\text{\AA}2$, indicating that the Gd valence state is unaffected by the surrounding nanotube.⁷

V. ACKNOWLEDGEMENTS

J.S. thanks the National Defense Science and Engineering Grant (NDSEG) program and U.S. Army Research Office Contract/Grant No. FDDAAD19-01-1-0612 for financial support. K.B.W. thanks the Miller Institute for Basic Research in Science for financial support. This work was also supported by the Defense Advanced Research Projects Agency (DARPA) and the Office of Naval Research under Grant No. FDN00014-01-1-0826, and the National Science Foundation under Grant EIA-020-1-0826. We thank the National Computational Science Alliance for partial support under the grant No. DMR030047.

¹ H. Shinohara, Rep. Prog. Phys. **63**, 843 (2000).

² D. Bethune, R. Johnson, J. R. Salem, M. Vries, and C. Yannoni, Nature **366**, 123 (1993).

³ J. Lee, H. Kim, S.-J. Kahng, G. Kim, Y.-W. Son, J. Ihm, H. Kato, Z. W. Wang, T. Okazaki, H. Shinohara, et al., Nature **415**, 1005 (2002).

⁴ K. Hirahara, K. Suenaga, S. Bandow, H. Kato, T. Okazaki, H. Shinohara, and S. Iijima, Phys. Rev. Lett. **85**, 5384 (2000).

- ⁵ T. Shimada, T. Okazaki, R. Taniguchi, T. Sugai, H. Shinohara, K. Suenaga, Y. Ohno, S. Mizuno, S. Kishimoto, and T. Mizutani, *Appl. Phys. Lett.* **81**, 4067 (2002).
- ⁶ A. Ardavan, M. Austwick, S. Benjamin, G. Briggs, T. J. S. Dennis, A. Ferguson, D. G. Hasko, M. Kanai, A. Khlobystov, B. Lovett, et al., *Phil. Trans. Roy Soc. London A.* **361**, 1473 (2003).
- ⁷ T. Okazaki, T. Shimada, K. Suenaga, Y. Ohno, T. Mizutani, J. Lee, Y. Kuk, and H. Shinohara, *Appl. Phys. A* **76**, 475 (2003).
- ⁸ K. Kobayashi and S. Nagase, *Chem. Phys. Lett.* **282**, 325 (1998).
- ⁹ K. Furukawa, S. Okubo, H. Kato, H. Shinohara, and T. Kato, *J. Phys. Chem. A* **107**, 10933 (2003).
- ¹⁰ H. Funasaka, K. Sakurai, Y. Oda, K. Yamamoto, and T. Takahashi, *Chem. Phys. Lett.* **232**, 273 (1995).
- ¹¹ H. Funasaka, K. Sugiyama, K. Yamamoto, and T. Takahashi, *J. Phys. Chem.* **99**, 1826 (1995).
- ¹² H. J. Huang, S. H. Yang, and X. X. Zhang, *J. Phys. Chem. B* **103**, 5928 (1999).
- ¹³ H. Huang, S. Yang, and X. Zhang, *J. Phys. Chem. B* **104**, 1473 (2000).
- ¹⁴ R. G. Parr and W. Yang, *Density-Functional Theory of Atoms and Molecules* (Oxford Science, Oxford, 1994).
- ¹⁵ A. Kant and S. S. Lin, *Monash. Chem.* **103**, 757 (1971).
- ¹⁶ M. Dolg, W. Liu, and S. Kalvoda, *Int. J. Quantum Chem.* **76**, 359 (2000).
- ¹⁷ T. R. Cundari and W. J. Stevens, *J. Chem. Phys.* **98**, 5555 (1993).
- ¹⁸ A. D. Becke, *J. Chem. Phys.* **98**, 5648 (1993).
- ¹⁹ C. Lee, W. Yang, and R. G. Parr, *Phys. Rev. B* **37**, 785 (1988).
- ²⁰ M. J. F. et al., *GAUSSIAN 03* (Gaussian Inc., Pittsburgh, PA, 2003).
- ²¹ A. Szabo and N. S. Ostlund, *Modern Quantum Chemistry* (Dover, Mineola, 1996).
- ²² R. Yerulshalmi, A. Scherz, and K. K. Baldrige, *J. Am. Chem. Soc.* **126**, 5897 (2004).
- ²³ A. E. Reed, R. B. Weinstock, and F. Weinhold, *J. Chem. Phys.* **83**, 735 (1985).
- ²⁴ S. Datta, *Electron Transport in Mesoscopic Systems* (Cambridge University Press, Cambridge, 1997).
- ²⁵ R. Pati, L. Senapati, P. M. Ajayan, and S. K. Nayak, *Phys. Rev. B* **68**, 100407 (2003).
- ²⁶ W. Tian, S. Datta, S. Hong, R. Reifenberger, J. I. Henderson, and C. P. Kubiak, *J. Chem. Phys.* **109**, 2874 (1998).
- ²⁷ J. P. Perdew and Y. Wang, *Phys. Rev. B* **45**, 13244 (1992).
- ²⁸ M. Takata, B. Umeda, E. Nishibori, M. Sakata, Y. Saito, M. Ohno, and H. Shinohara, *Nature* **377**, 46 (1995).
- ²⁹ E. Nishihori, M. Takata, M. Sakata, H. Tanaka, M. Hasegawa, and H. Shinohara, *Chem. Phys. Lett.* **330**, 497 (2000).
- ³⁰ E. Nishihori, M. Takata, M. Sakata, M. Inakuma, and H. Shinohara, *Chem. Phys. Lett.* **298**, 79 (1998).
- ³¹ K. Kobayashi and S. Nagase, in *Endohedralfullerenes: A New Family of Carbon Clusters*, edited by T. Akasaka and S. Nagase (Kluwer, Dordrecht, 2002), pp. 99–119.
- ³² K. Kobayashi and S. Nagase, *Mol. Phys.* **101**, 249 (2003).

- ³³ E. Nishibori, K. Iwata, M. Sakata, M. Takata, H. Tanaka, H. Kato, and H. Shinohara, *Phys. Rev. B* **69**, 113412 (2004).
- ³⁴ K. Suenaga, S. Iijima, H. Kato, and H. Shinohara, *Phys. Rev. B* **62**, 1627 (2000).
- ³⁵ R. H. Crabtree, *The Organometallic Chemistry of the Transition Metals* (Wiley-Interscience, New York, 1994), 2nd ed.
- ³⁶ C. D. Nadai, A. Mirone, S. S. Dhesi, P. Bencok, N. B. Brookes, I. Marenne, P. Rudolf, N. Tagmatarchis, H. Shinohara, and T. J. S. Dennis, *Phys. Rev. B* **69**, 184421 (2004).
- ³⁷ F. A. Cotton, G. Wilkinson, C. A. Murillo, and M. Bochmann, *Advanced Inorganic Chemistry* (Wiley-Interscience, New York, 1999), sixth ed.
- ³⁸ S. Pagliara, L. Sangaletti, C. Cepek, F. Bondino, R. Larciprete, and A. Goldoni, *Phys. Rev. B* **70**, 035420 (2004).
- ³⁹ S.-H. Ke, H. U. Baranger, and W. Yang, cond-mat/0402409.

TABLE I: Calculated total energies and binding energies for the optimized structures of $\text{\textcircled{8}2}$ and $\text{Gd@}\text{\textcircled{8}2}$ as a function of Gd spin multiplicity, M . The $M=7$ state of $\text{Gd@}\text{\textcircled{8}2}$ is found to be 2.6 meV below the $M=9$ state in total energy.

$Atom(M)$	$TE(au)$	$BE(eV)$
$\text{\textcircled{8}2}(C_{2v})$	-3123.805927	
$\text{Gd@}\text{\textcircled{8}2}(M=5)$	-3235.8783289	4.4066
$\text{Gd@}\text{\textcircled{8}2}(M=7)$	-3235.9237819	5.6435
$\text{Gd@}\text{\textcircled{8}2}(M=9)$	-3235.9236904	5.6409
$\text{Gd@}\text{\textcircled{8}2}(M=11)$	-3235.87890696	4.4224

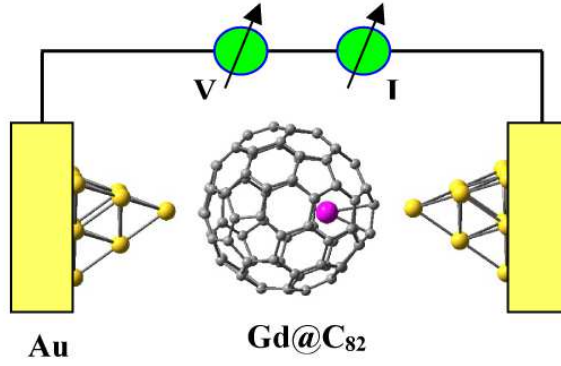


FIG. 1: Gold contact model used for transport calculations across $\text{Gd@}\text{\textcircled{8}2}$ (see part b). The first layer adjacent to $\text{\textcircled{8}2}$ has one Au atom, the second has 3 Au atoms and the third layer has 6 Au atoms.

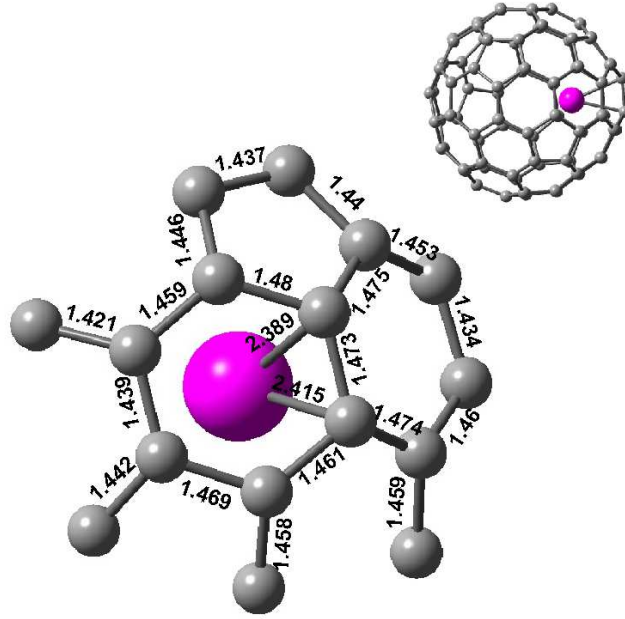


FIG. 2: Optimized structure of Gd@82. The ground state structure of Gd@82 has the Gd atom (purple) situated adjacent to the C-C double bond on the C_{2v} symmetry axis that connects a six-membered ring with a C=C bond on the other side of the fullerene. The distances between Gd and the two nearest C atoms are 2.38 Å and 2.41 Å respectively. The lines between Gd and C are used to indicate the closest carbon atoms.

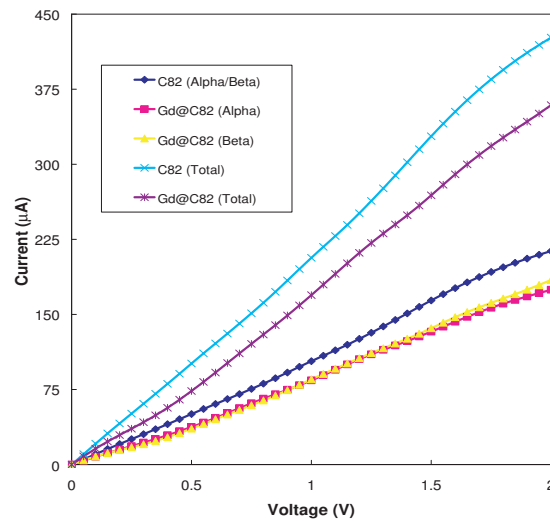


FIG. 3: I-V plot for single Au atom contacts. Total conduction (sum of spin up and spin down conduction) for Gd@82 is lower at all bias voltages than for pure fullerene 82. Conduction of spin up (alpha) and spin down (beta) electrons is similar at all bias values.

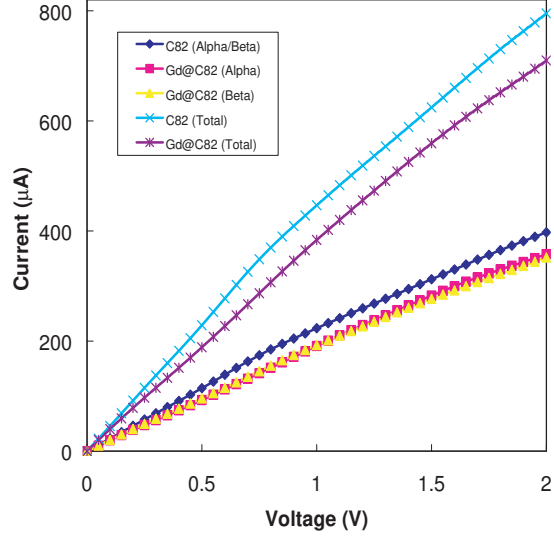


FIG. 4: I-V plot for contact geometry shown in Figure 1. Note the qualitative similarity to the other contact geometries (Figs. 3, Supplement Fig. 2).

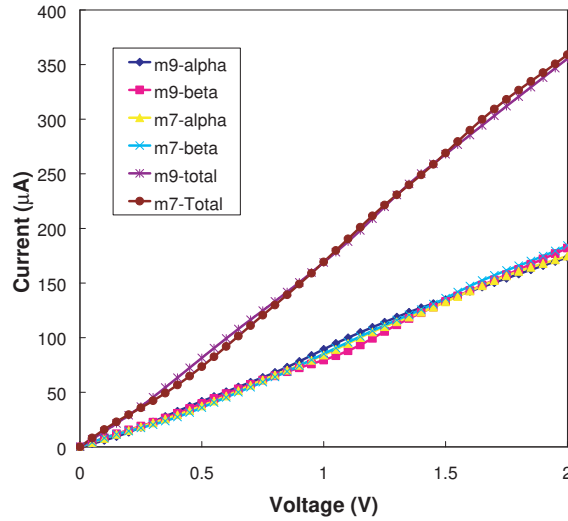


FIG. 5: I-V plot for conduction in the spin multiplicity $M=7$ ground state, and the $M=9$ state with energy 2.6 meV higher in energy. Conduction characteristics for spin polarized and unpolarized currents are similar for both cases, with neither showing strong spin-dependent transport effects. This suggests that the current is mainly carried through the §2 cage, and does not involve the Gd atom.

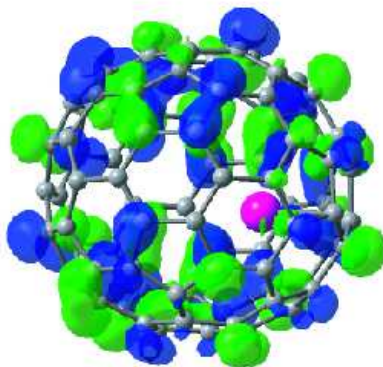


FIG. 6: Lowest Unoccupied Molecular Orbital (LUMO) plot of $\text{Gd}@C_{82}$ showing localization on the C_{82} cage without significant LUMO orbitals on the Gd atom. Blue and green are used to indicate the positive and negative sign of the wavefunction, respectively. The purple sphere indicated the Gd atom.

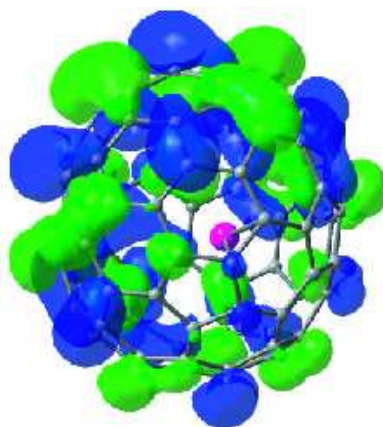


FIG. 7: Highest Occupied Molecular Orbital (HOMO) plot of $\text{Gd}@C_{82}$. Blue and green are used to indicate the positive and negative sign of the wavefunction. HOMO orbitals are localized on cage of C_{82} and there is no HOMO orbital on Gd (purple sphere). From both HOMO and LUMO plots, it is evident that the current is mainly carried through the C_{82} cage, as opposed to the Gd atom.